Effects of Rain on Propagation, Absorption and Scattering of Microwave Radiation Based on the Dielectric Model of Liebe

Christian Mätzler

Research Report No. 2002-10
June 2002

Institut für Angewandte Physik Mikrowellenabteilung

Sidlerstrasse 5
3012 Bern
Schweiz

Tel. : +41 31 631 89 11
Fax. : +41 31 631 37 65
E-mail : matzler@iap.unibe.ch

Effects of Rain on Propagation, Absorption and Scattering of Microwave Radiation Based on the Dielectric Model of Liebe

Christian Mätzler, Institute of Applied Physics, University of Bern, June 2002

List of Contents

Abstract

This report presents results from Mie computations for extinction, scattering, absorption, backscattering, asymmetry parameter and angular scattering behaviour of microwave radiation by rain, based on a recently developed MATLAB software, and using two versions of the dielectric model of water by Liebe. The results are also quantitatively compared with results from Rayleigh Theory. The report contains the code of the MATLAB routines.

1 Introduction

Mie Theory (Mie, 1908), known for almost one century, allows for exact modelling of wave propagation, absorption and scattering characteristics of spheres and of clouds of such particles, provided that the dielectric and magnetic properties of the particle are known. Water droplets of rain and clouds are nearly spherical, homogeneous, dielectric particles, thus Mie Theory is quite appropriate for applications in atmospheric physics. Mie Theory has also been widely used for this purpose (e.g. Deirmendjian, 1969) to complement the results of Rayleigh scattering which are a much simpler formulation, but applicable for small size parameters ($x=ak<<1$, a= drop radius, k= wave number) only. Most published studies usually relied on old dielectric data, such as Ray (1972) - being especially inaccurate at frequencies above 10 GHz - and often the studies of Mie scattering were incomplete descriptions by considering one or another aspect, only; e.g. Olsen et al. (1978) gave a quantitative description of extinction by rain. Olsen's result were of recent interest (Mätzler 2002a) to quantify rain effects on radar signals.

A useful set of parameters, allowing a larger range of applications (wave propagation, radiometer, monostatic radar), must include the extinction γ_{ext}, absorption γ_{abs}, and backscattering coefficient γ_b, respectively, including the scattering coefficient γ_{sca} from γ_{ext}-γ_{abs}; in addition, for modelling radiometer data with radiative transfer theory the full phase matrix is required as well or at least the asymmetry parameter $g=\langle\cos\theta\rangle$ if a simplified method is applied, such as the few-stream models (Meador and Weaver, 1980). These parameters are computed and plotted by a set of MATLAB Functions, developed by Mätzler (2002b), based on the book of Bohren and Huffman (1983). The present report is an application of this software. The objective is threefold:

1. to extend the MATLAB functions to cloud and rain applications for general use in the 1 to 1000 GHz range (or to the optical range with an appropriate refractive model of water),
2. to prepare our research group for microwave radiometry of the rainy atmosphere,
3. to replace the rather inaccurate results of Olsen et al. (1978) by better ones and to complement them with more additional information.

Here, the presently assumed standard dielectric model of water will be applied (Liebe et al. 1991), and comparisons will be made with an alternative one (Liebe et al. 1993). At a temperature of 300K, the two models coincide. They deviate just in one parameter, the permittivity at infinite frequency,

$$\varepsilon_\infty = \begin{cases} 3.52 + 7.52\theta; & \text{Liebe et al.(1991)} \\ 3.52\ ; & \text{Liebe et al.(1993)} \end{cases} \tag{1}$$

where θ =1-300/T, and T is the temperature in K. Thus at frequencies f near or below 30 GHz, the difference between the two models is negligible.

The Marshall and Palmer (MP) drop-size distribution will be assumed:

$$N_{MP}(D) = N_0 \exp(-\Lambda D) \tag{2}$$

with the drop diameter D, the parameter Λ being given by (Sauvageot, 1992)

$$\Lambda = 3.67/D_0 = 41R^{-0.21} \qquad (1/cm) \tag{3}$$

where D_0 (cm) is the median diameter, R (mm/h) the rain rate, and N_0 = 0.08 cm^{-4}. Olsen et al. (1978) and de Wolf (2001) proposed renormalisations of the MP distri-

bution to produce correct rain rates. Since these corrections are different, we will omit them here.

2 Single water droplets

2.1 Mie Efficiencies

Mie Theory requires the complex refractive index of water m as input parameter. Since the relative magnetic permeability of water is very close to 1, we can assume the relationship for non-magnetic materials

$$m = \sqrt{\varepsilon} \tag{4}$$

where ε is the complex relative dielectric constant (or permittivity) of liquid water. For ε we use the model of Liebe et al. (1991). The MATLAB function is called epswater. For the alternative model, Liebe et al. (1993), the MATLAB Function is called epswater93.
Mie Efficiencies of water droplets are computed at T=277K for two frequencies, using the MATLAB Function Mie_rain1. The results are shown versus drop diameter D in Figures 1 and 2. At the logarithmic scales, starting at D=10μm (a typical cloud-drop size), the figures emphasise the Rayleigh regime with straight lines up to about 2 mm at 5 GHz and 0.3 mm at 94 GHz. This is the reason why rain-radar data at 5 GHz (e.g. Sauvageot, 1992) are usually interpreted in terms of Rayleigh scattering theory (van de Hulst, 1957, Ishimaru, 1978).

2.2 Comparison with Rayleigh Theory

To test the accuracy of the Rayleigh Approximation, the Mie and Rayleigh results are compared in Figure 3. It is observed that Rayleigh Theory underestimates absorption at f=5GHz at D=2mm (x≅0.1) by a factor of 1/2 already, and computations with an accuracy of 10% only reach to D=0.7 mm. For accurate modelling of microwave emission, absorption should be known to the 1% level. Thus Mie Theory is needed in microwave radiometry of rain at 5 GHz and at all higher frequencies.
For scattering and backscattering, on the other hand, the Rayleigh Approximation is valid (deviations < 25%) up to D=6 mm, thus covering the full range of rain drops. Since radar data are usually needed with an accuracy of about 1 dB (26%), the Rayleigh Approximation is sufficient for radar observations at 5 GHz. Note the slightly oscillatory behaviour of the Mie backscattering efficiency around the Rayleigh curve in Figure 3.
Similar results are found at 94 GHz (bottom graph of Figure 3). The underestimate of absorption of the Rayleigh curve by a factor of 1/2 is reached at D=0.5 mm (x≅0.5), i.e. at a 4 times lower value of D than at 5 GHz, whereas the frequency is higher by a factor of 19. This behaviour is due to the relaxation spectrum of water. Again for scattering, and especially for backscattering, the Rayleigh Approximation is useful up to higher D values, about 0.8 mm.

2.3 Comparison between Liebe'91 and Liebe'93

The two dielectric models, Liebe et al. (1991) and Liebe et al. (1993), give slightly different results. The difference increases with increasing frequency and with temperature decreasing from 300 K. Mie efficiencies and their differences between the two dielectric models at 277K are shown in Figure 4 for f=24 and 220 GHz, respec-

tively. The differences are well below 0.001 at 24 GHz, whereas the efficiencies are on the order of 1. At 220 GHz, on the other hand, the differences

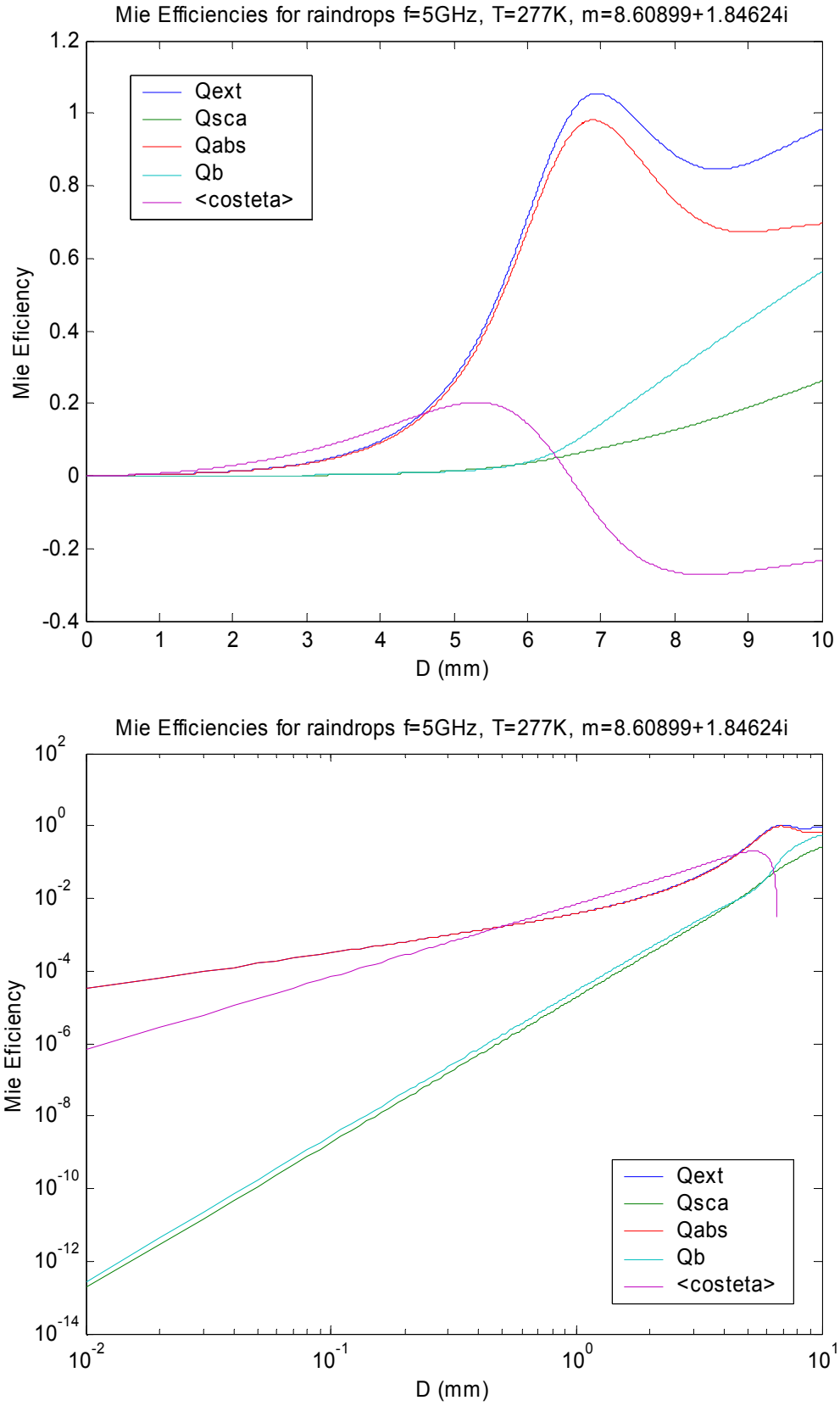

Figure 1: Mie efficiencies of cloud and rain drops versus drop diameter at T=277K, f=5 GHz, linear scale (top), logarithmic scale (bottom).

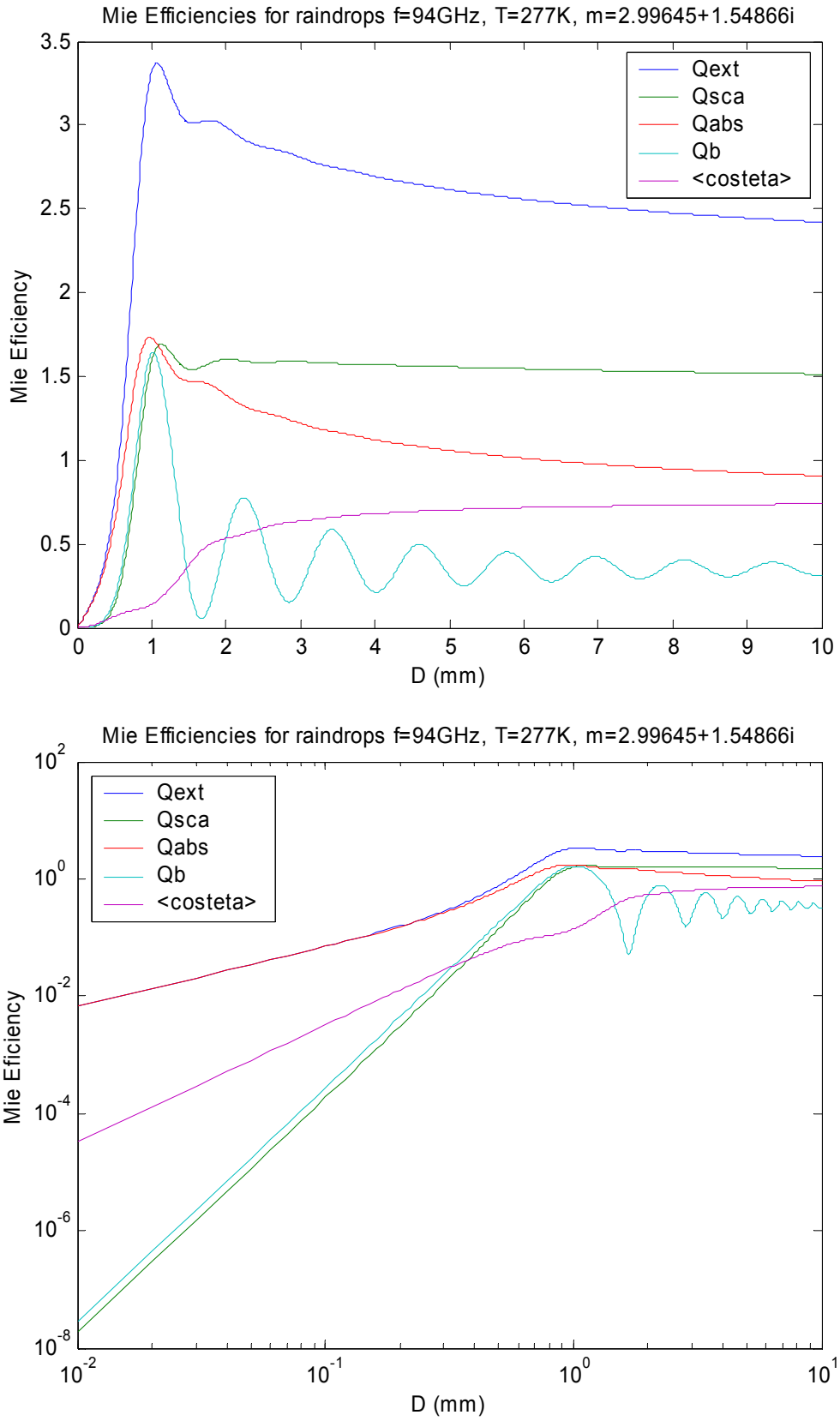

Figure 2: Mie efficiencies of cloud and rain drops versus drop diameter at T=277K, f=94 GHz, linear scale (top), logarithmic scale (bottom).

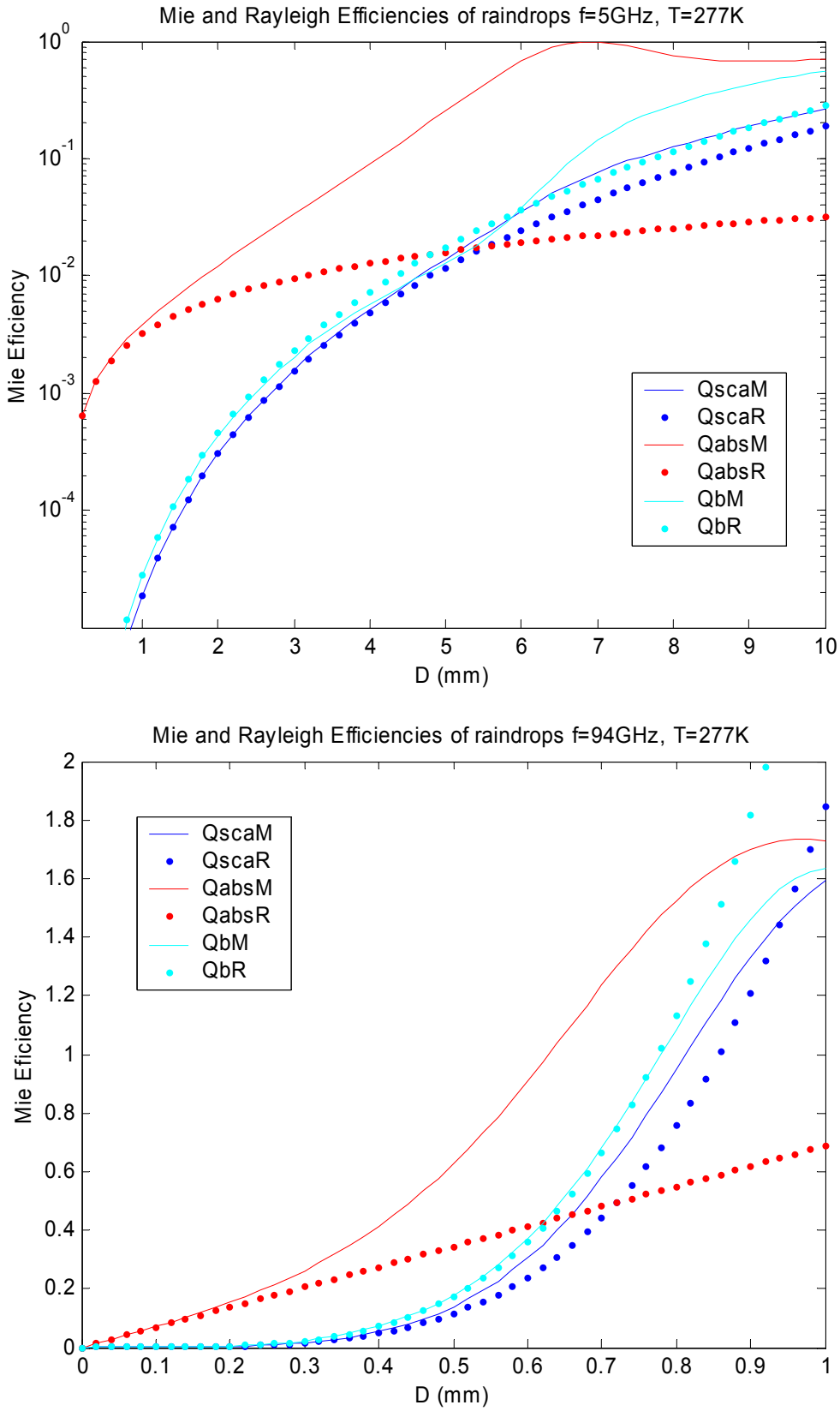

Figure 3: Mie Efficiencies of water drops versus drop diameter in Mie (M) and Rayleigh (R) Theory at T=277K, f= 5 (top) and 94 GHz (bottom), respectively.

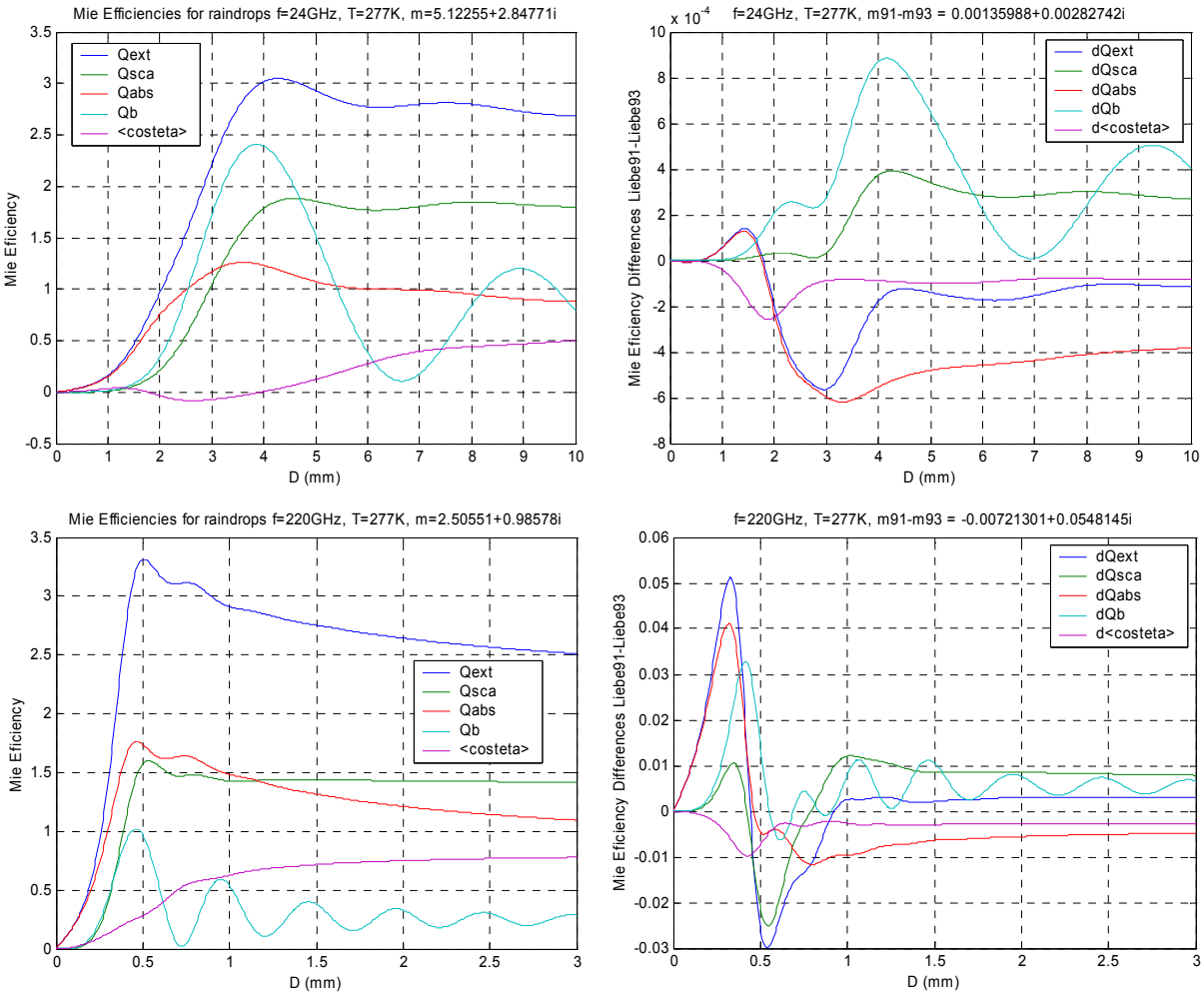

Figure 4: Mie Efficiencies at 24 (upper left) and 220 GHz (lower left) versus drop diameter at T=277K, and (right) the differences between the two dielectric models, Liebe et a. (1991) – Liebe et al. (1993).

are on the order of 0.01, reaching up to 0.05. Still these differences do not deviate by more than 1% or a few %. Therefore, from here on, we will neglect the differences between the two models, by using Liebe'91 only.

2.5 Angular diagrams and the internal field

Scattering diagrams of water droplets with increasing D are shown for f=94 GHz in the graphs of Figure 5. While the scattering efficiency is nearly constant at about 1.6 for the three situations (s. Figure 2), there is a strong change from near-isotropic scattering at x=1 to forward scattering at x=2.2. This change is indicated in Figure 2 by the increase of <cosθ> over the considered range of x. The top graph of Figure 5 is the situation with maximum backscattering Q_b, the middle graph shows a situation with reduced Q_b, and the bottom graph corresponds to the second maximum of Q_b in Figure 2. While the monostatic radar signal from rain is not directly influenced by the changing scattering diagram, the modeling of microwave emission depends on the angular diagram, i.e. on the phase function (Chandrasekhar, 1960; Ishimaru, 1978).

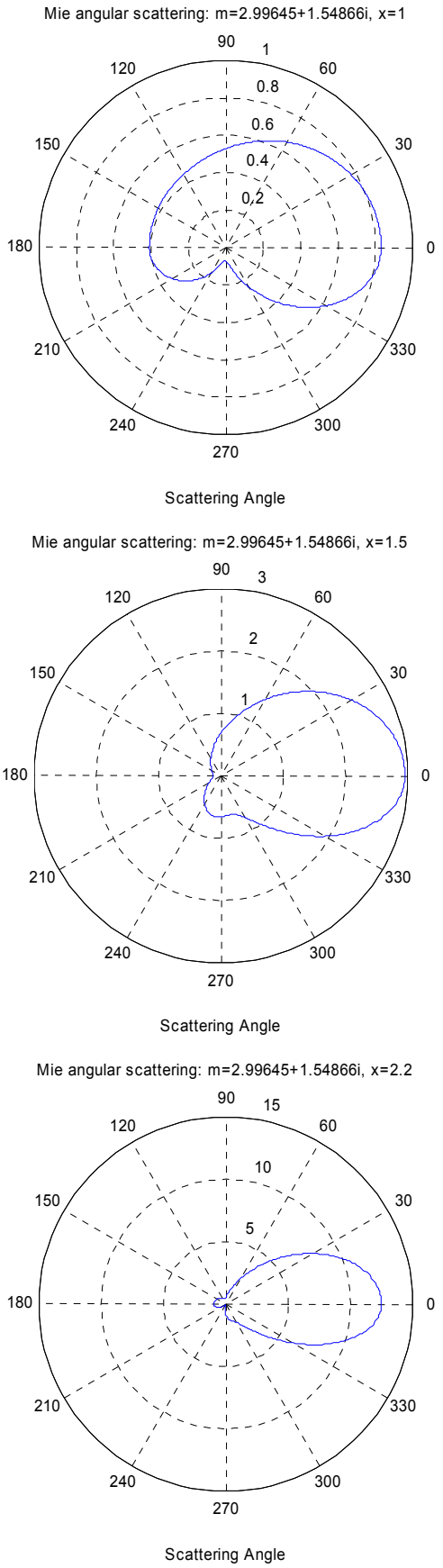

Figure 5: Angular diagrams for Mie scattering on raindrops at f=94 GHz, T=277K, top: x=1 (D=1.02 mm), middle: x=1.5 (D=1.52 mm), bottom: x=2.2 (D=2.23 mm).

The upper part of the curves (angular range 0-180°) are for polarization perpendicular to the scattering plane, and the lower part of the curves (angular range 180-360°) are for polarization parallel to the scattering plane.

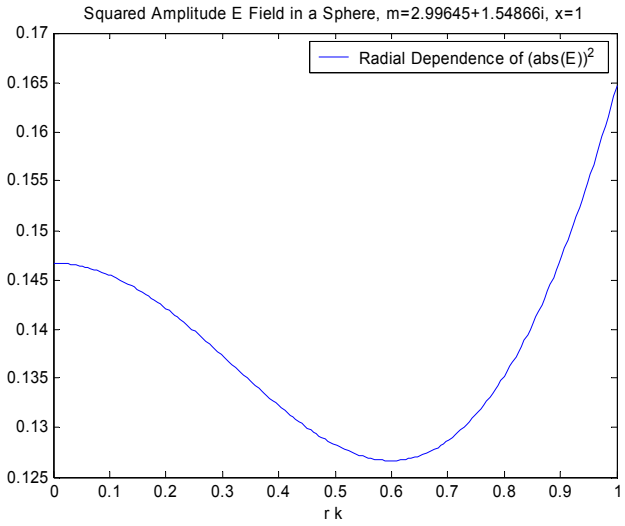

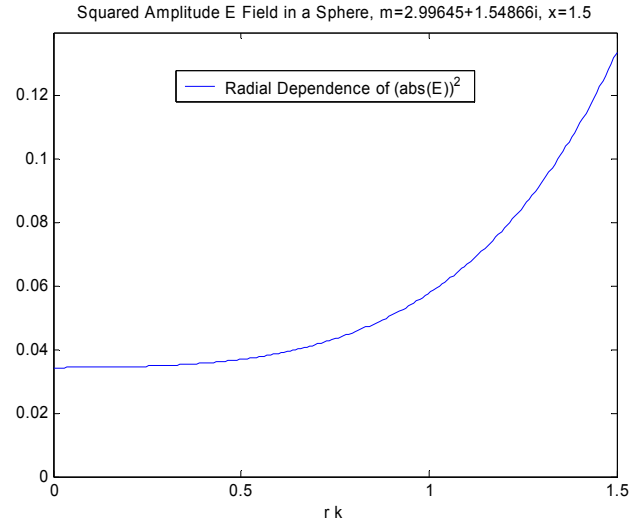

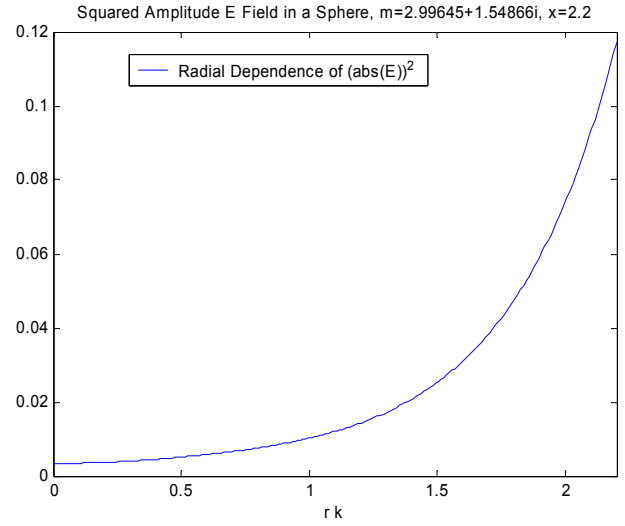

Figure 6: Radial dependence of mean-absolute-square electric field ratio between inside a raindrop and the incident field for Mie scattering at f=94 GHz, T=277K,
top: x=1 (D=1.02 mm),
middle: x=1.5 (D=1.52 mm),
bottom: x=2.2 (D=2.23 mm).

The ratio of the absolute-square electric field between the inside of the sphere and the incident field is shown here in the graphs of Figure 6 versus the k-normalised radial distance r for the 3 situations of Figure 5. The values are averaged over shells of constant radius.
It is seen that already at x=1 the internal field is significantly larger than in case of Rayleigh scattering; in the Rayleigh limit, the value follows from $9/\left|m^2+2\right|^2$, thus becomes 0.056. This is the reason for the enhanced absorption in Mie Theory for small values of x (here x=1).
At the bottom graph, the field is concentrated at the edge of the drop due to the skin effect.

3 Clouds of rain drops

3.1 Transformation from efficiencies to coefficients

For a large number of independently and incoherently scattering rain drops distributed in air (assuming the refractive index of air being 1), the propagation coefficients (extinction γ_{ext}, scattering γ_{sca}, backscattering γ_b and absorption γ_{abs} coefficients) are determined from the Mie efficiencies and the drop-size distribution by

$$\gamma_j = 0.25\pi \int_0^\infty D^2 Q_j(D) N_{MP}(d) dD \;\; ; \quad j = ext,\ abs,\ sca,\ b \tag{5}$$

$$\gamma_{sca} \langle \cos\theta \rangle = 0.25\pi \int_0^\infty D^2 < \cos\theta > (D) \cdot Q_{sca}(D) N_{MP}(d) dD \tag{6}$$

where <cosθ>(*D*) is a function of *D*; the dimension of the coefficients is 1/(length) as they represent densities of cross sections. Here we will use 1/km or, what is identical, neper/km. The transformation to dB/km is obtained by multiplying the γ_j values with $10 \cdot {}_{10}\log e \cong 0.4342$. These coefficients are used in radiative transfer theory (Chandrasekhar, 1960, Meador and Weaver, 1980).

3.2 Weighting functions of coefficients

The integrands of γ_j can be considered as weighting functions in the averaging over *D*. The strong exponential decrease of N_{MP} with increasing *D* gives a strong weighting of small droplets. On the other hand, the efficiencies of zero-sized droplets are zero and increase, according to the Rayleigh Approximation, in proportion to D^2 for absorption and D^6 for scattering. Thus, there is a *D* range of maximum influence, depending on the parameter in question, and with a strong sensitivity to frequency. Different situations are shown in the following figures, based on the MATLAB Function Mie_rain2. At frequencies up to 10 GHz, scattering is negligible in comparison to absorption. An example with *f*=5 GHz is shown in Figure 7. To better see the scattering effects, logarithmic scales are used in Figure 8, showing data at 10 and 18 GHz.

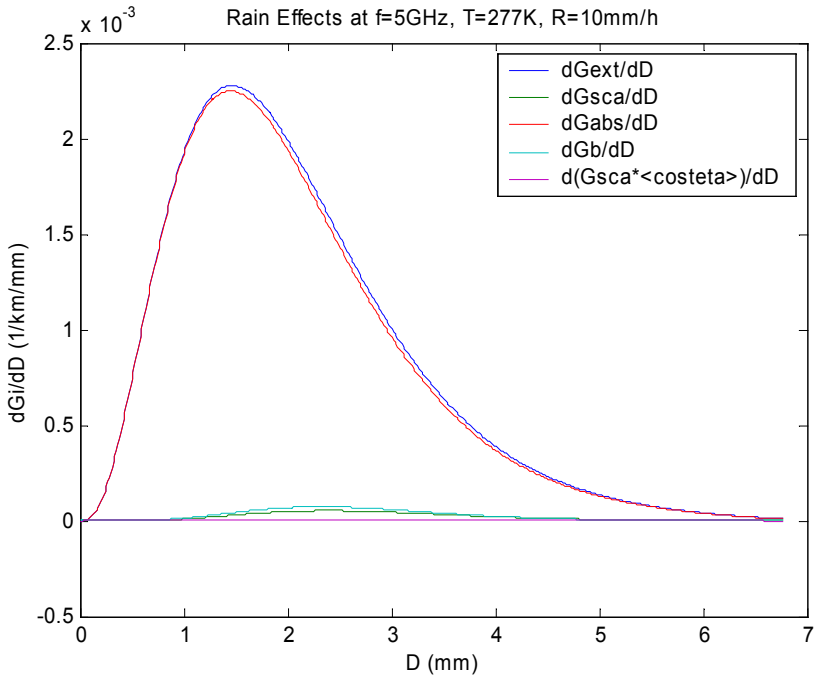

Figure 7:
Integrands of γ_j at *f*=5 GHz, *T*=277K.

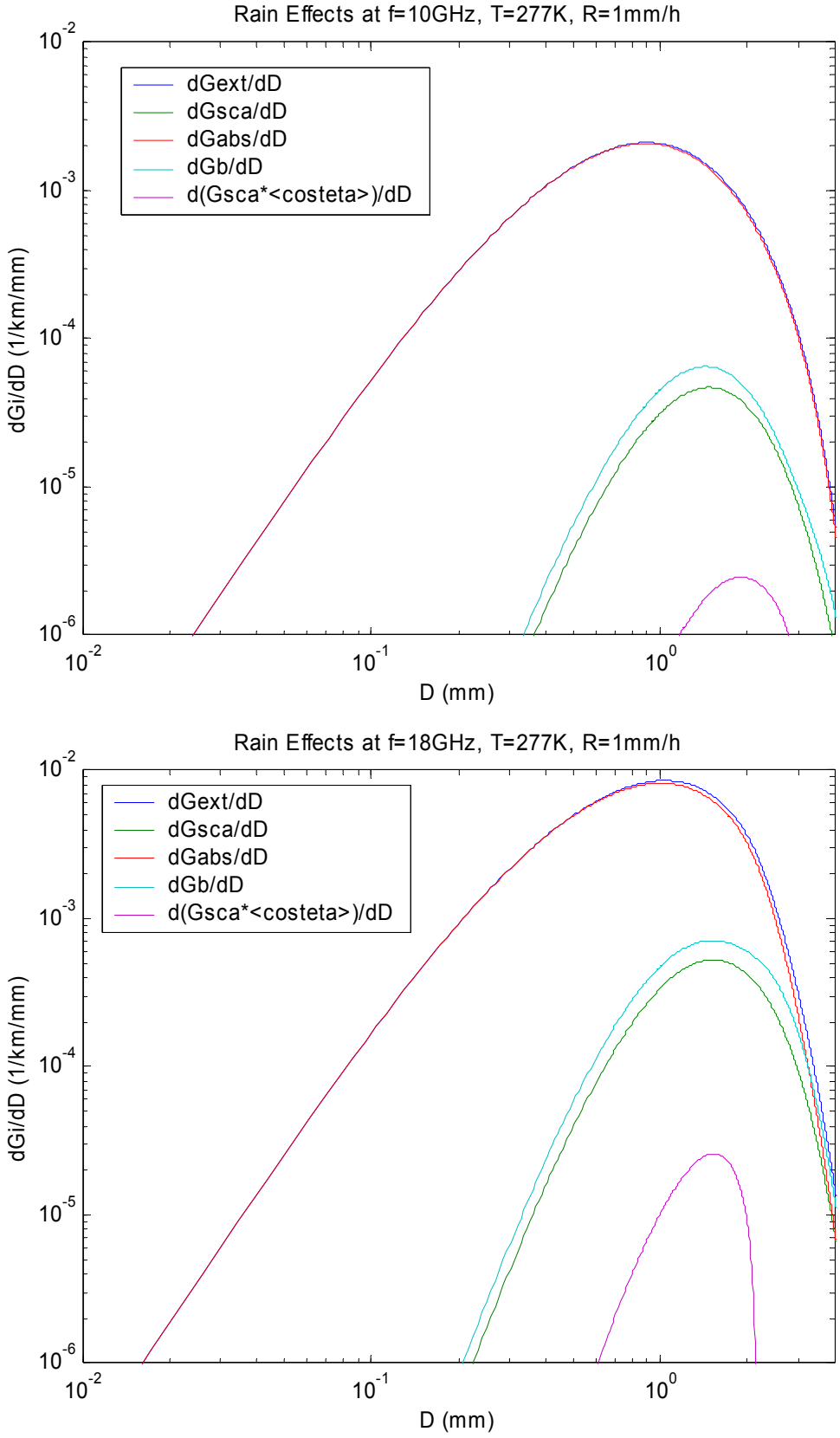

Figure 8: Integrands of extinction γ_{ext}, scattering γ_{sca}, absorption γ_{abs}, and backscattering coefficients γ_b, and of $\gamma_{sca}\langle\cos\theta\rangle$, versus drop diameter D in logarithmic scales at T=277K, f=10 GHz (top) and 18 GHz (bottom) for Marshall-Palmer drop-size distribution.

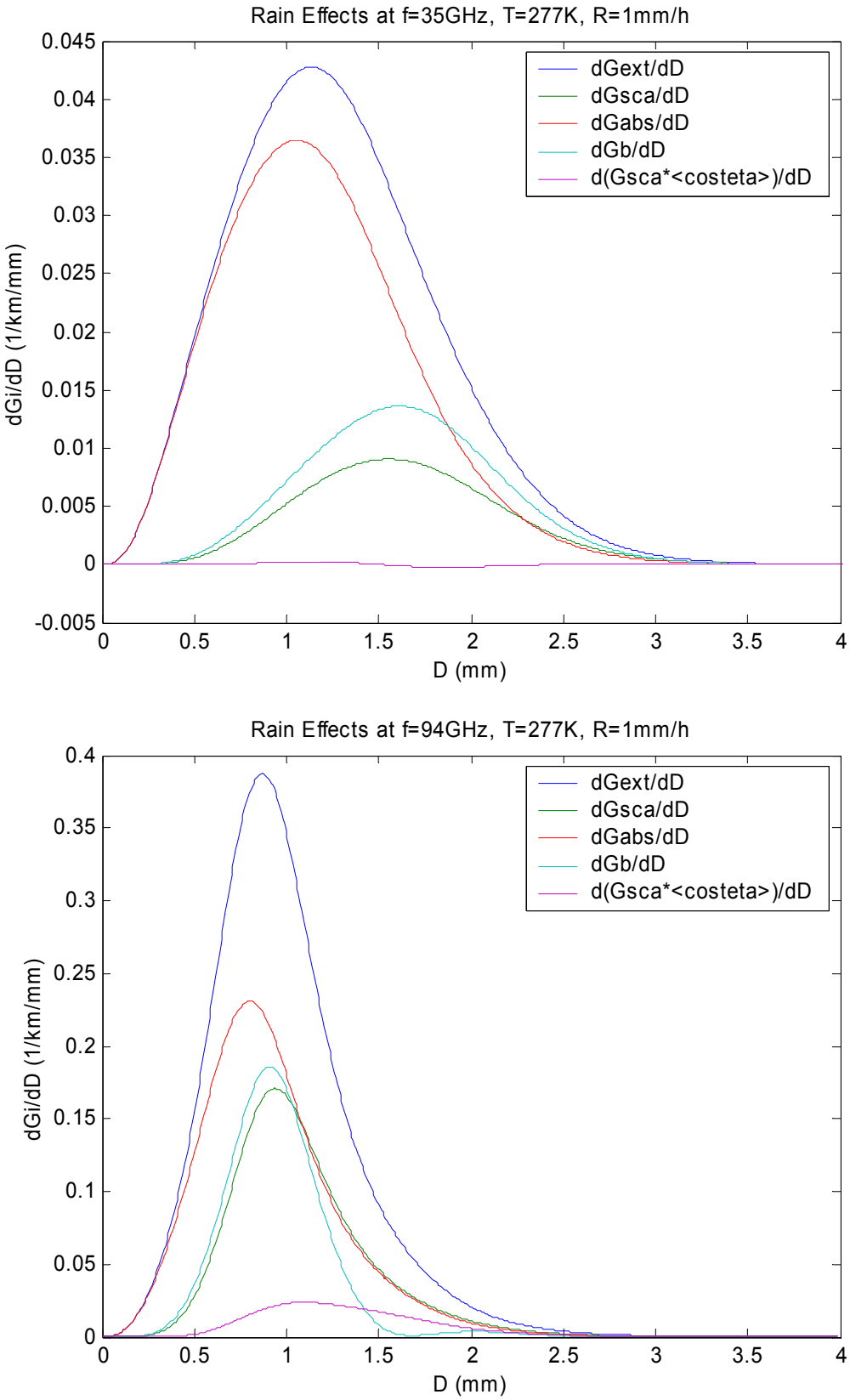

Figure 9: Integrands of extinction γ_{ext}, scattering γ_{sca}, absorption γ_{abs}, and backscattering coefficients γ_b, and of $\gamma_{sca}\langle\cos\theta\rangle$, versus drop diameter D at T=277K, f=35 GHz (top) and 94 GHz (bottom) for Marshall-Palmer drop-size distribution.

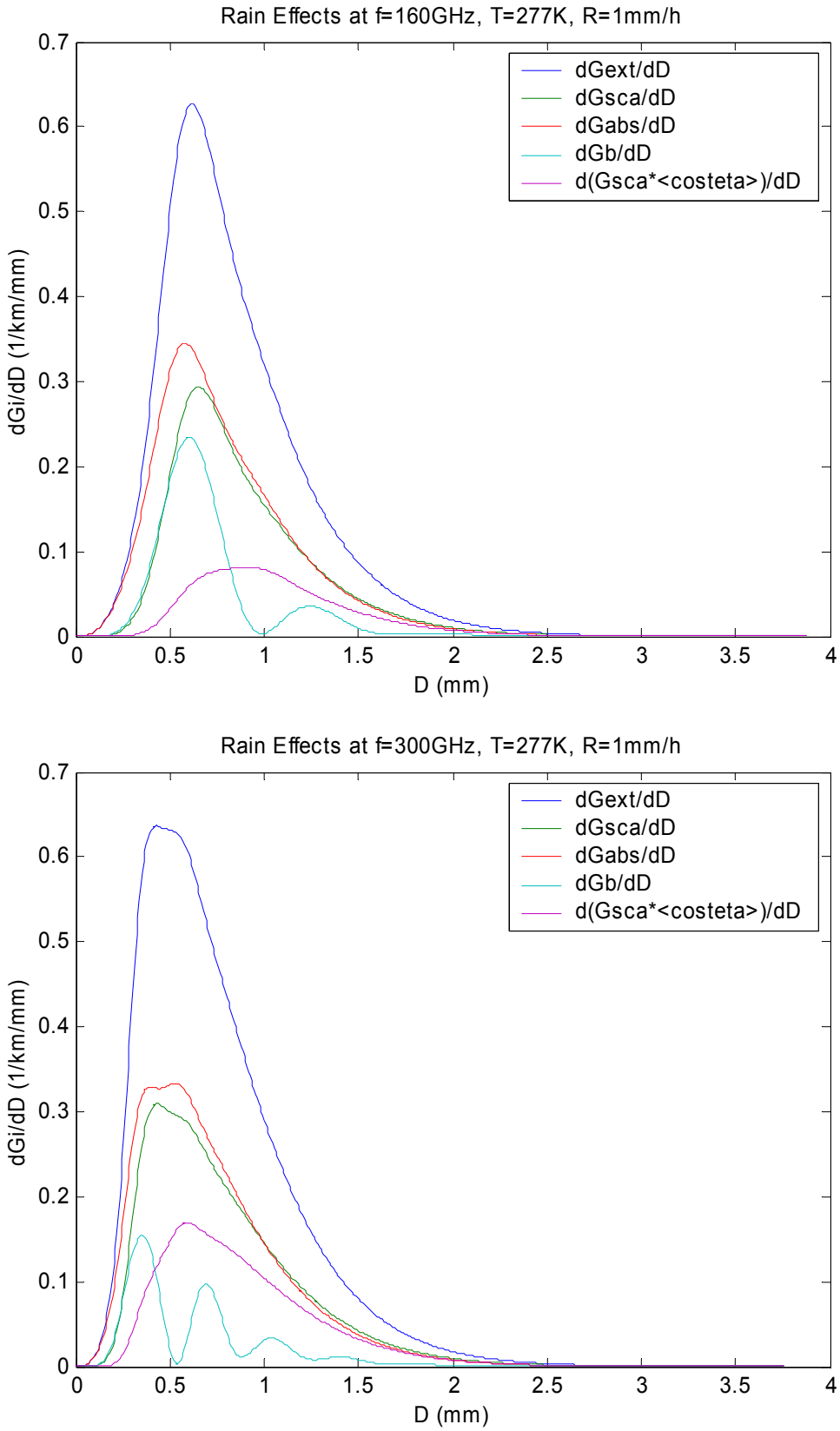

Figure 10: Integrands of extinction γ_{ext}, scattering γ_{sca}, absorption γ_{abs}, and backscattering coefficients γ_b, and of $\gamma_{sca}\langle\cos\theta\rangle$, versus drop diameter D at T=277K, f=160 GHz (top) and 300 GHz (bottom) for Marshall-Palmer drop-size distribution.

Figures 9 and 10, again with linear scales, represent the behaviour at frequencies from 31 to 300 GHz. It is interesting to note that the functions shown in Figures 7 to 10 are clearly peaked ones. This is especially true for the backscattering coefficient γ_b. It means that a multi-frequency radar can give detailed information on the drop-size distribution. Reasons why radar systems have - so far - not been used for this purpose, may be related to the inherent noise (e.g. speckle, clutter) in the data, and in the high extinction at mm wavelengths.
The maximum of the weighting for γ_b is near D=2.2 mm at 5 GHz, almost constant near 1.5 mm at 10 to 35 GHz, at 1mm near 94 GHz, at 0.6 mm at 160 GHz and 0.3 mm at 300 GHz. Thus the typical drop-size range is covered by these frequencies. Note that the weighting functions of other parameters are slightly different. The asymmetry parameter has sometimes slightly negative values, indicating increased scattering in the backward hemisphere. But more often the values are positive.

3.3 Rain spectra

The results of the integration of the Mie Efficiencies over the drop-size distribution leads to the propagation coefficients, using the MATLAB Function Mie_rain3. Care has to be taken to select the best range of D values. The following parameters were found to be useful and to give accurate results with trapezoidal integration:

$$\text{nsteps=501; dD=0.01*R\^{}(1/6)/fGHz\^{}0.05;} \qquad (7)$$

where nsteps is the number of steps in the numerical integration, starting at D=0, and dD is the increment in dependence on rain rate R(mm/h) and frequency fGHz (GHz).
The γ_j spectra of rain at 277K are shown in Figure 11 for rain rates R of 1 and 10 mm/h. These curves tend to increase with increasing frequency, either reaching saturation at the top or above the presented spectral range or a flat peak, especially for γ_b. The peak frequency decreases with increasing rain rate. Another feature is the decreasing dominance of absorption with increasing frequency and rain rate.

3.4 Rain-rate dependence

The γ_j coefficients are shown versus rain rate, both in linear and logarithmic scales in Figures 12 to 17. These are quite smooth curves in both representations, sometimes being almost straight lines.
The extinction coefficients can be used to check the approximate formula of Olsen et al. (1978), $\gamma_{ext} \cong \alpha R^{\beta}$, where α and β depend on frequency, drop-size distribution and temperature. For T=0, 10 and 20C, and for the dielectric water model of Ray (1972), these parameters were given by Olson et al. (1978), and the tables are reprinted by Mätzler (2002a). However, when looking at Figures 12 to 17, it is clear that the Olsen formula cannot be very accurate as it require strait lines in the logarithmic representations. Therefore Olsen's fits represent rough approximations of extinction, only.

3.4 Temperature dependence

The dependence of the propagation coefficients on temperature is shown by Figures 18 to 20, covering the frequency range, 5 to 94 GHz. The maximum sensitivity is found for absorption at the lowest frequency; this is a result of the rather strong temperature dependence of the lower relaxation frequency.

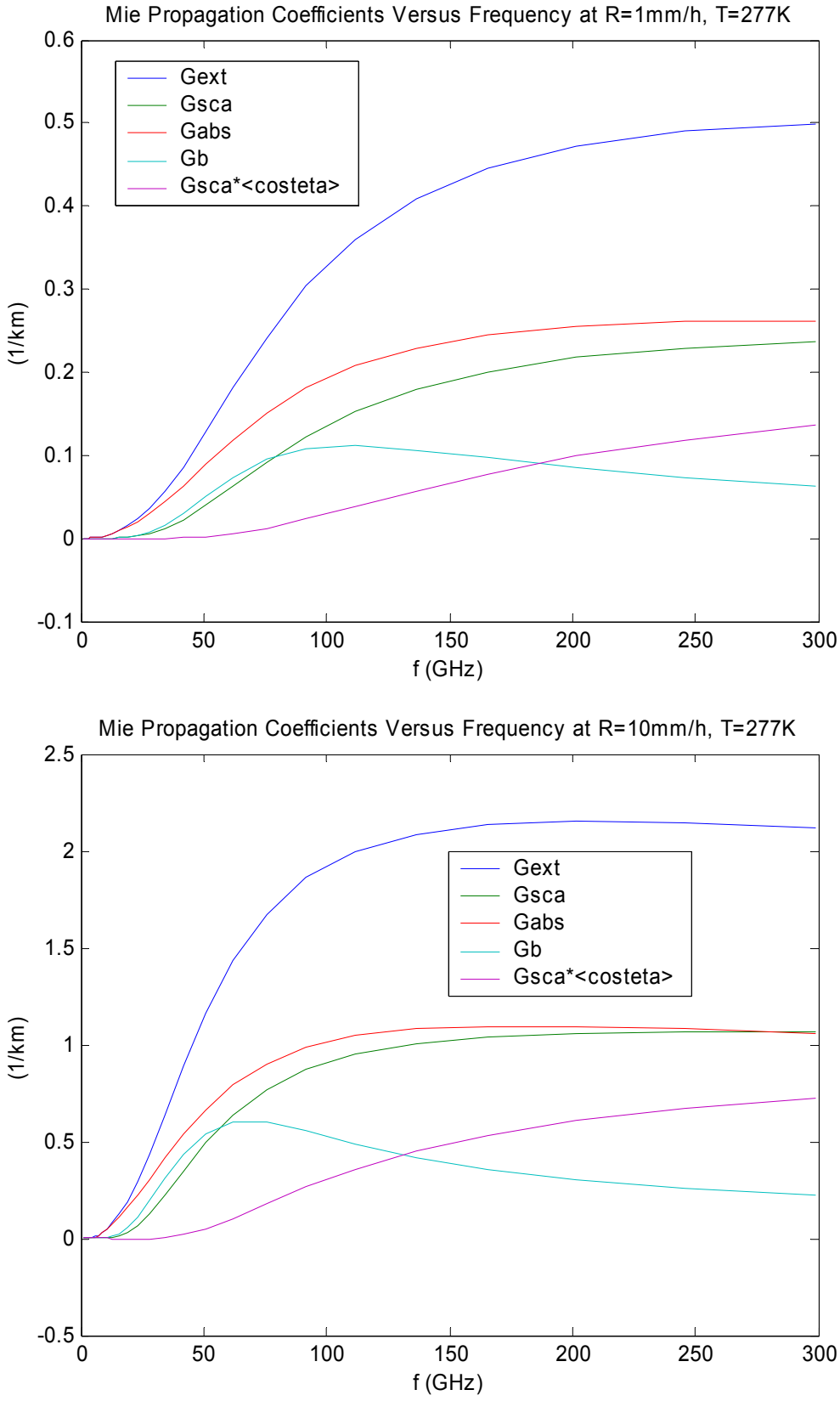

Figure 11, top: Extinction coefficient γ_{ext}, scattering coefficient γ_{sca}, absorption coefficient γ_{abs}, backscattering coefficient γ_b, and $\gamma_{sca}\cdot\langle\cos\theta\rangle$ versus frequency at the rain rate of 1mm/h, T=277K, for Marshall-Palmer drop-size distribution; bottom: Same, but for rain rate of 10 mm/h.

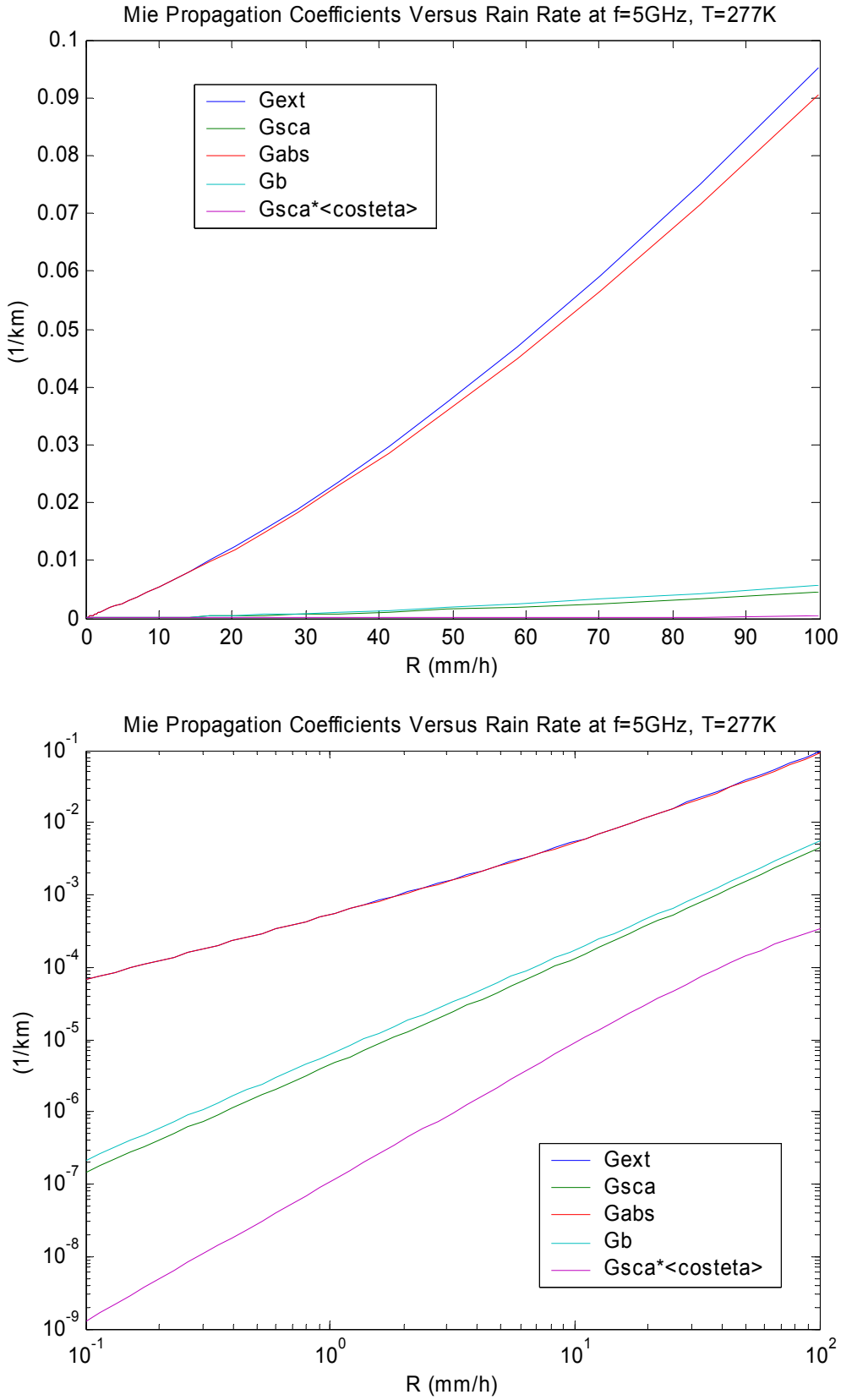

Figure 12, top: Extinction coefficient γ_{ext}, scattering coefficient γ_{sca}, absorption coefficient γ_{abs}, backscattering coefficient γ_b, and $\gamma_{sca}\cdot\langle\cos\theta\rangle$ versus rain rate at T=277K, f=5GHz for Marshall-Palmer drop-size distribution. Linear scales; bottom: Same, but logarithmic scales.

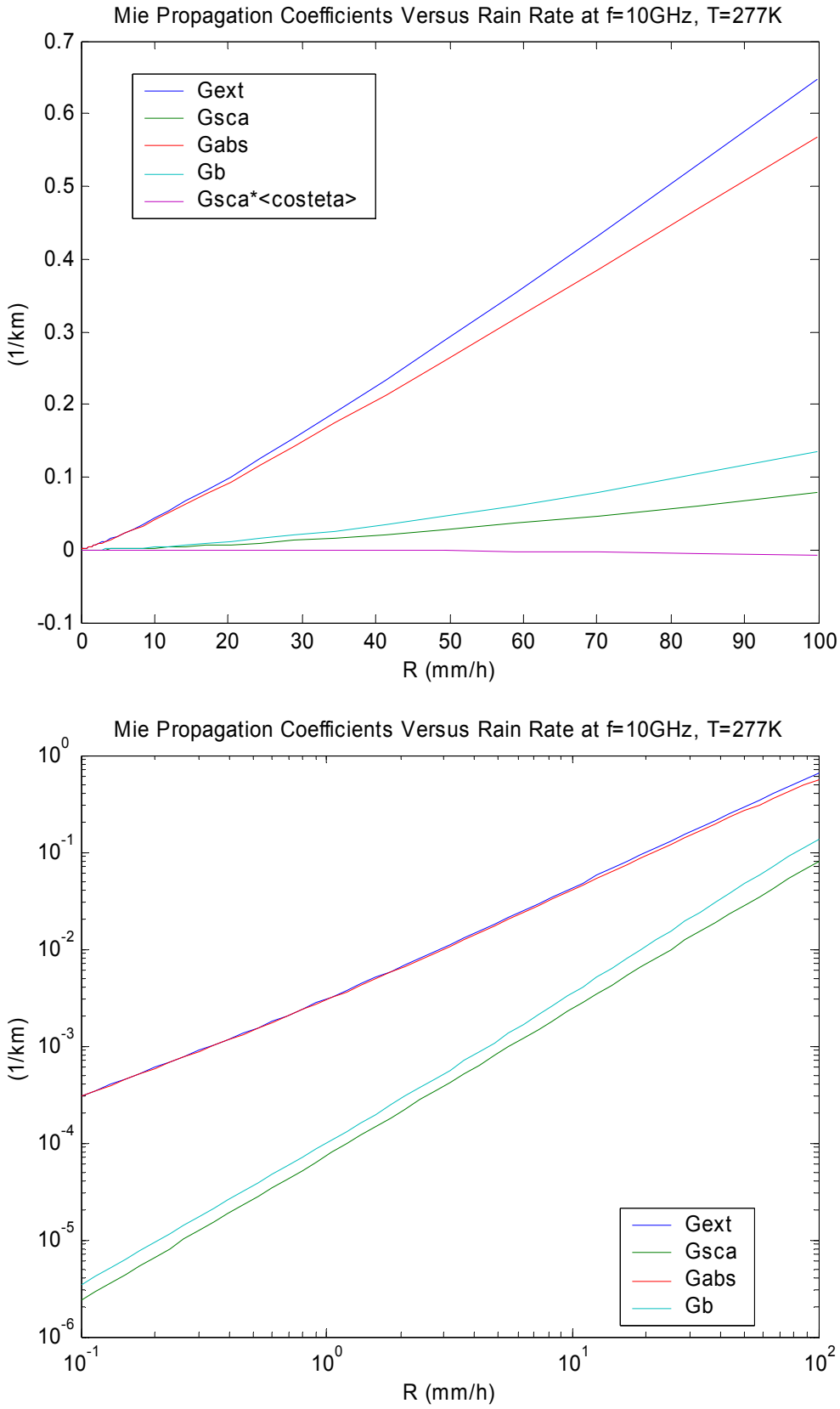

Figure 13, top: Extinction coefficient γ_{ext}, scattering coefficient γ_{sca}, absorption coefficient γ_{abs}, backscattering coefficient γ_b, and $\gamma_{sca}\cdot\langle\cos\theta\rangle$ versus rain rate at T=277K, f=10GHz for Marshall-Palmer drop-size distribution. Linear scales; bottom: Same, without $\gamma_{sca}\cdot\langle\cos\theta\rangle$, logarithmic scales.

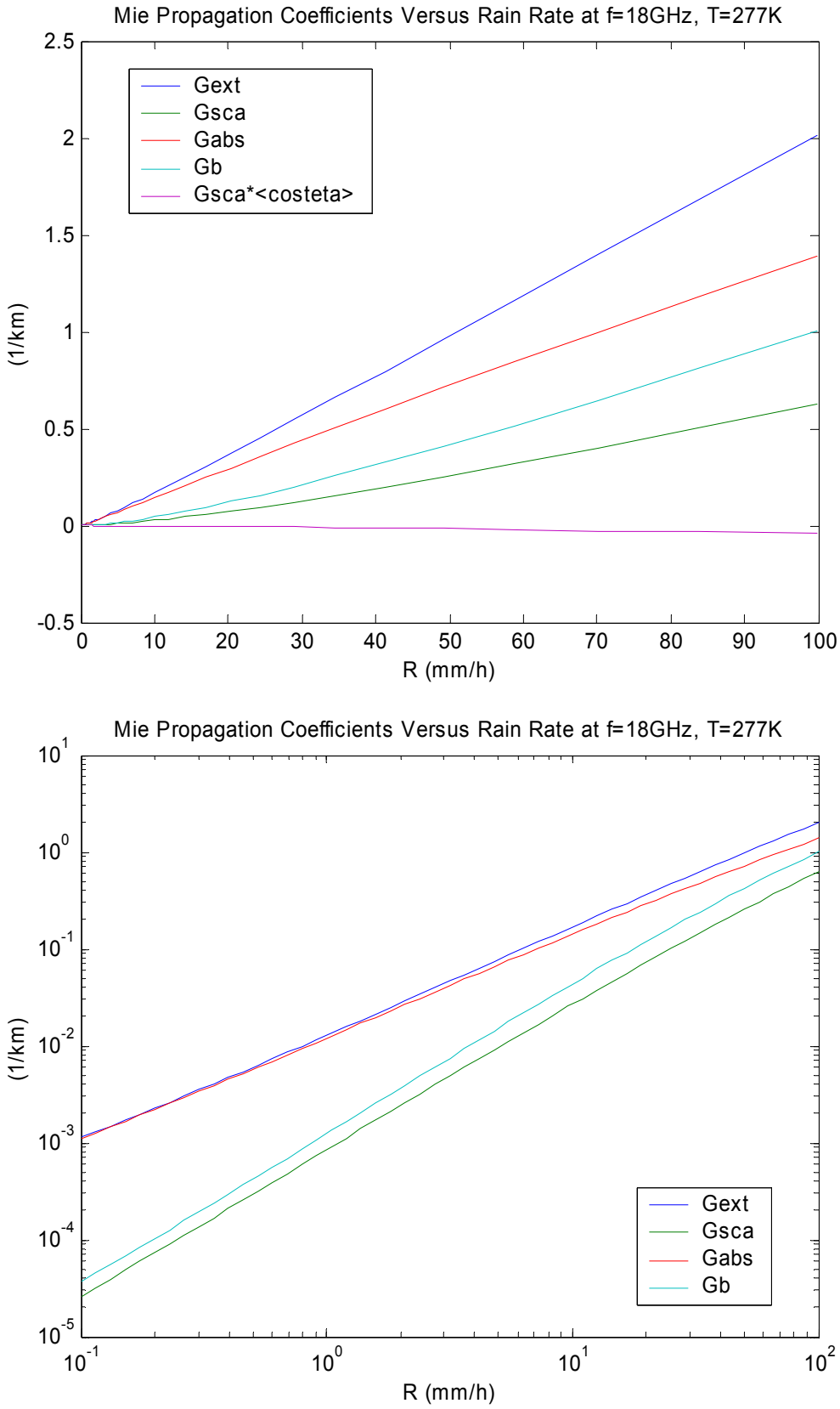

Figure 14, top: Extinction coefficient γ_{ext}, scattering coefficient γ_{sca}, absorption coefficient γ_{abs}, backscattering coefficient γ_b, and $\gamma_{sca}\cdot\langle\cos\theta\rangle$ versus rain rate at T=277K, f=18GHz for Marshall-Palmer drop-size distribution. Linear scales; bottom: Same, without $\gamma_{sca}\cdot\langle\cos\theta\rangle$, logarithmic scales.

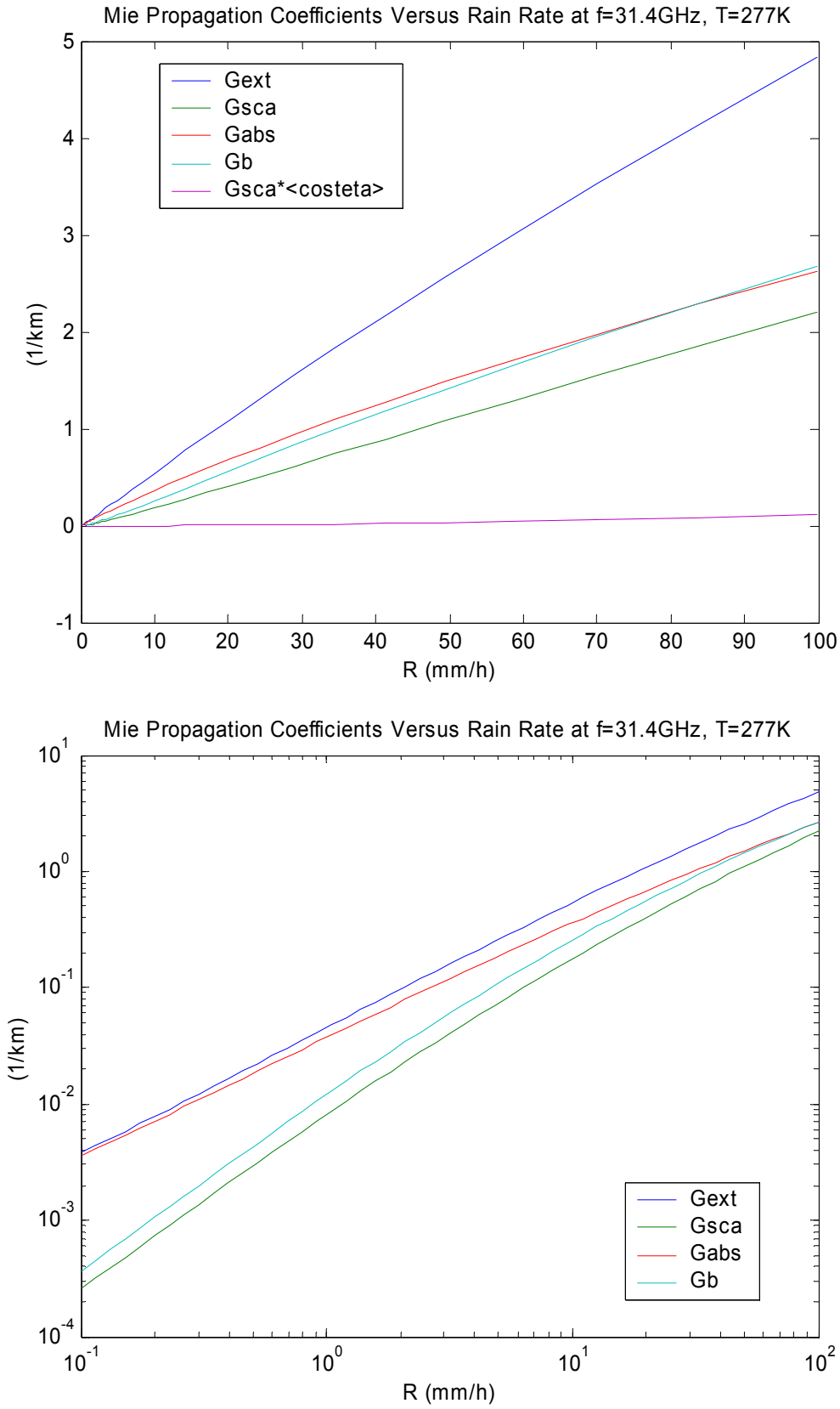

Figure 15, top: Extinction coefficient γ_{ext}, scattering coefficient γ_{sca}, absorption coefficient γ_{abs}, backscattering coefficient γ_b, and $\gamma_{sca}\cdot\langle\cos\theta\rangle$ versus rain rate at T=277K, f=31.4GHz for Marshall-Palmer drop-size distribution. Linear scales; bottom: Same, without $\gamma_{sca}\cdot\langle\cos\theta\rangle$, logarithmic scales.

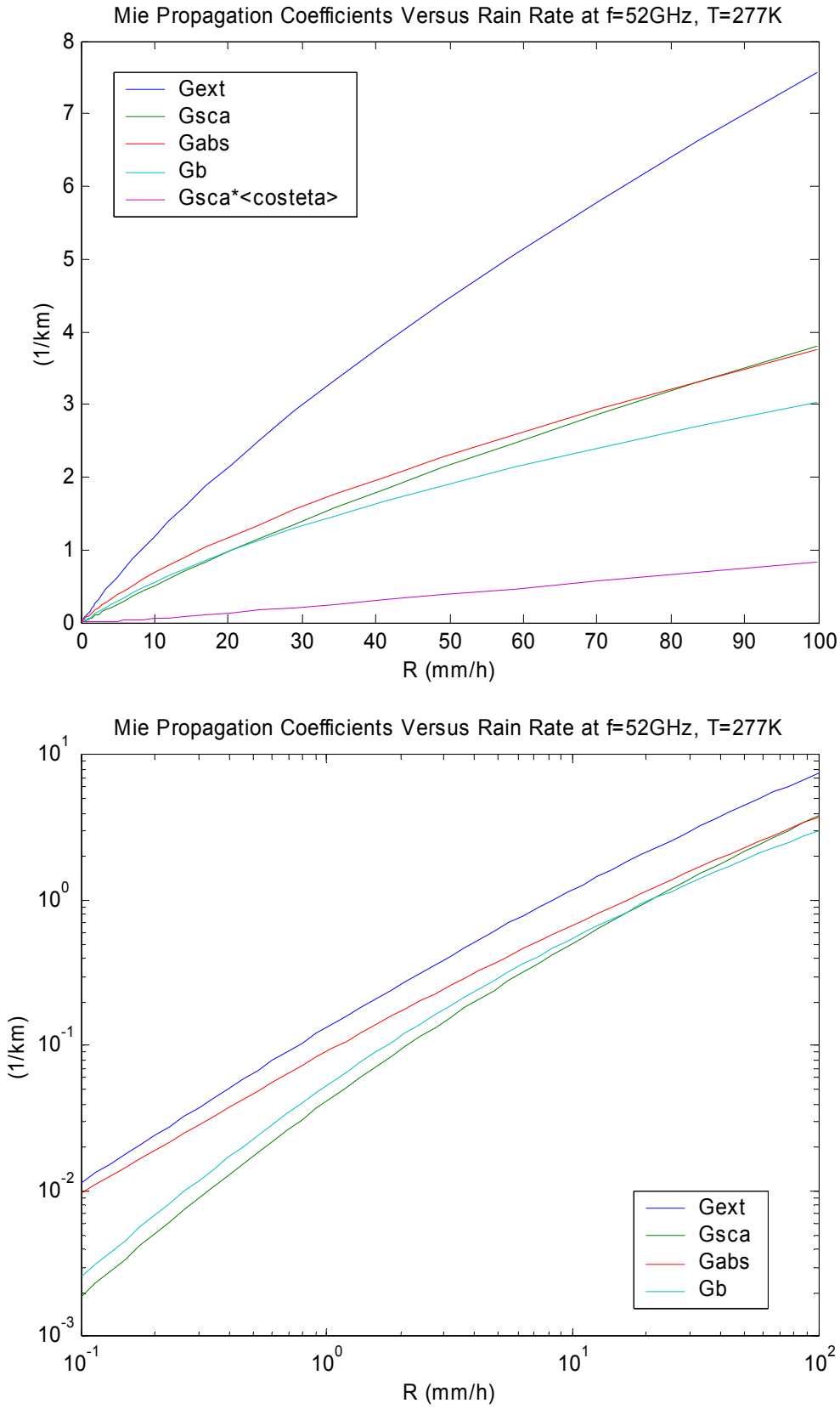

Figure 16, top: Extinction coefficient γ_{ext}, scattering coefficient γ_{sca}, absorption coefficient γ_{abs}, backscattering coefficient γ_b, and $\gamma_{sca}\cdot\langle\cos\theta\rangle$ versus rain rate at T=277K, f=52 GHz for Marshall-Palmer drop-size distribution. Linear scales; bottom: Same, without $\gamma_{sca}\cdot\langle\cos\theta\rangle$, logarithmic scales.

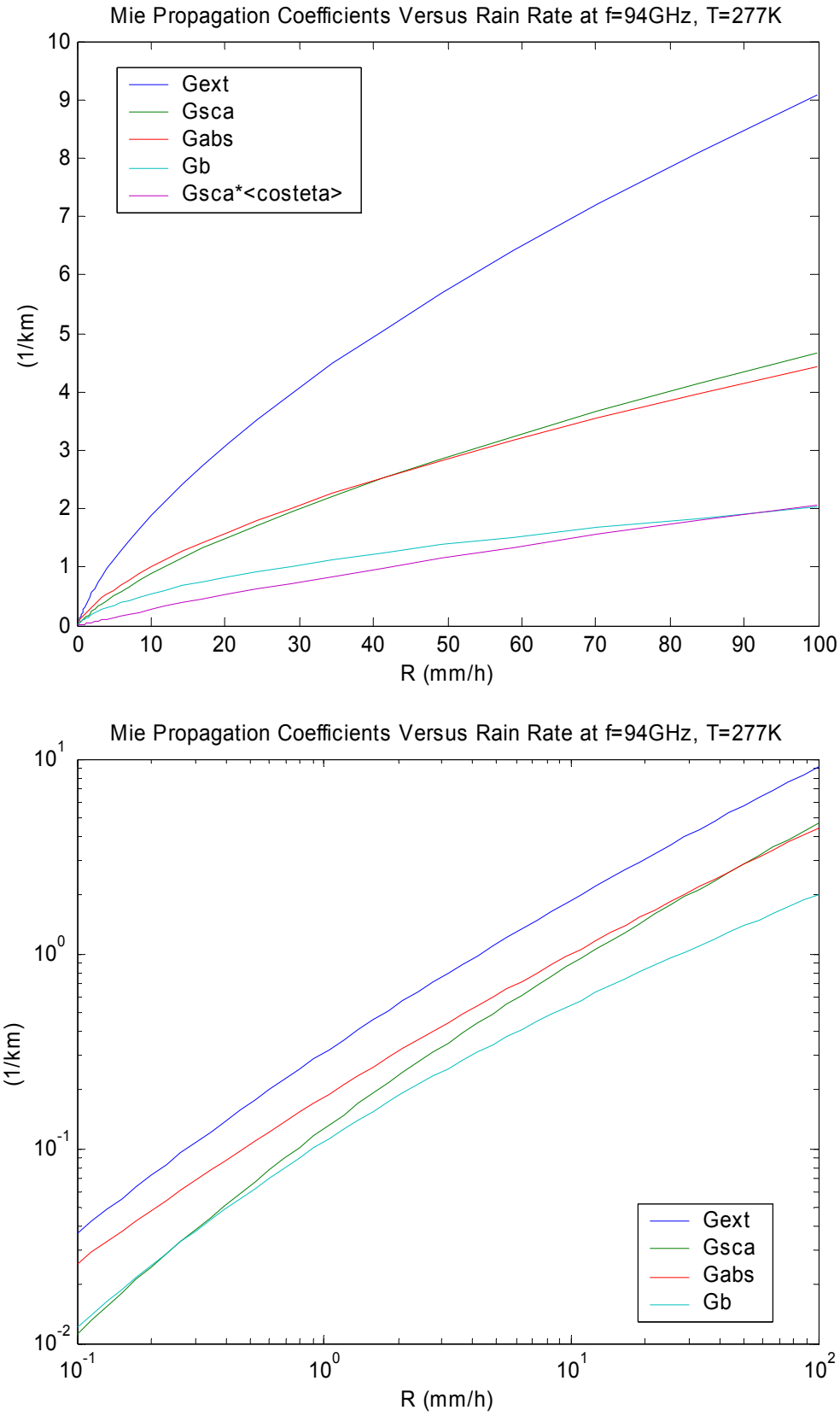

Figure 17, top: Extinction coefficient γ_{ext}, scattering coefficient γ_{sca}, absorption coefficient γ_{abs}, backscattering coefficient γ_b, and $\gamma_{sca}\cdot\langle\cos\theta\rangle$ versus rain rate at T=277K, f=94GHz for Marshall-Palmer drop-size distribution. Linear scales; bottom: Same, without $\gamma_{sca}\cdot\langle\cos\theta\rangle$, logarithmic scales.

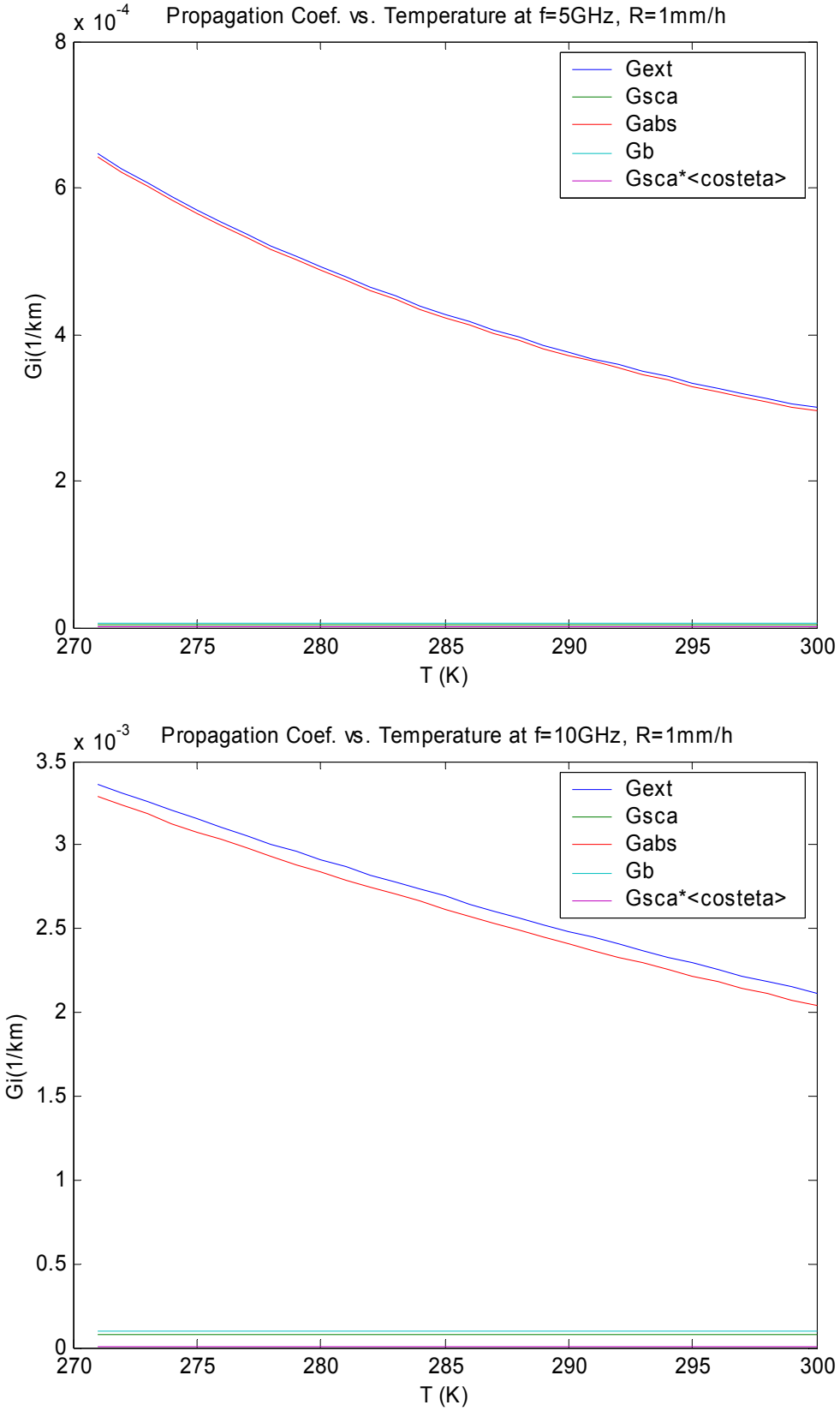

Figure 18: Extinction coefficient γ_{ext}, scattering coefficient γ_{sca}, absorption coefficient γ_{abs}, backscattering coefficient γ_b, and γ_{sca}·<cosθ> versus temperature for Marshall-Palmer drop-size distribution at R =1 mm/h, f=5 GHz top, f=10 GHz bottom.

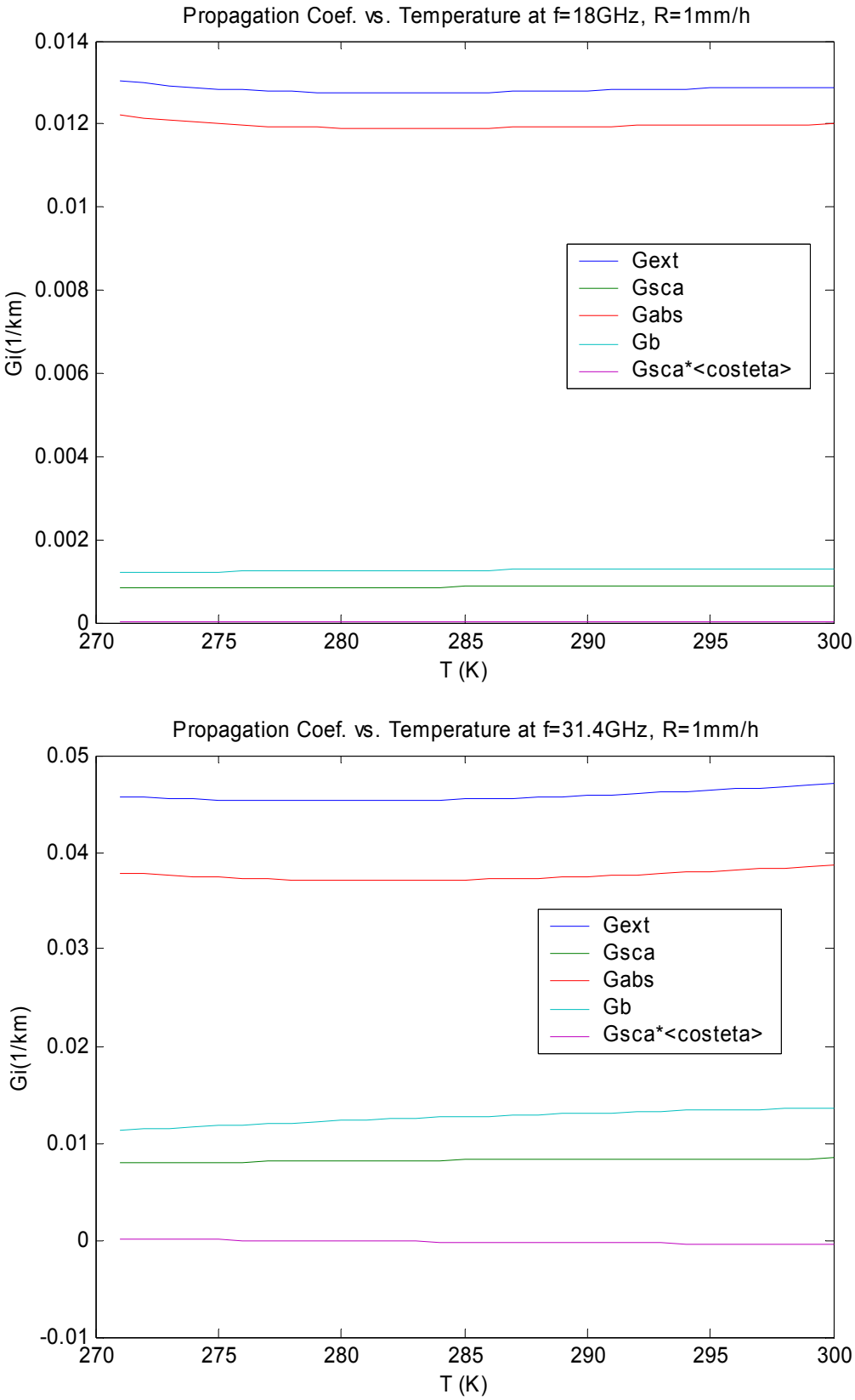

Figure 19: Extinction coefficient γ_{ext}, scattering coefficient γ_{sca}, absorption coefficient γ_{abs}, backscattering coefficient γ_b, and γ_{sca}·<cosθ> versus temperature for Marshall-Palmer drop-size distribution at R =1 mm/h, f=18 GHz top, f=31.4 GHz bottom.

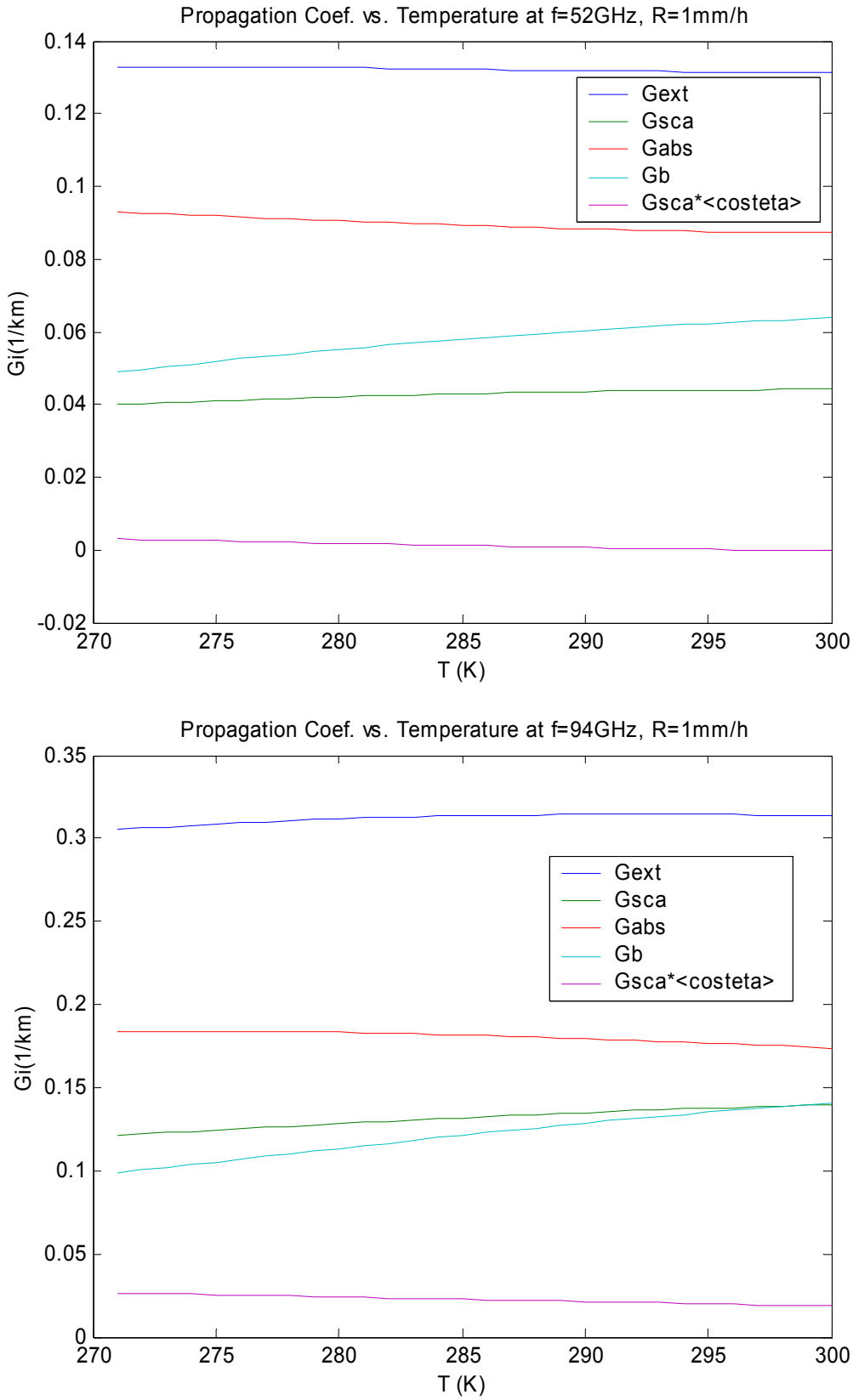

Figure 20: Extinction coefficient γ_{ext}, scattering coefficient γ_{sca}, absorption coefficient γ_{abs}, backscattering coefficient γ_b, and γ_{sca}·<cosθ> versus temperature for Marshall-Palmer drop-size distribution at R =1 mm/h, f=52 GHz top, f=94 GHz bottom.

4 Conclusions

This report is a graphical presentation of results from Mie Theory of rain in the microwave and millimeter wavelength range. The presentation is as comprehensive as possible by giving all relevant parameters and showing all relevant dependencies. The graphs are instructive in the sense that they show how the different parameters behave, how they are related quantitatively and which drop-sizes contribute most. In addition, the results show that the limits of Rayleigh Theory are not just at a size parameter of x=1, as often stated. The absorption coefficient can be strongly underestimated by the Rayleigh Approximation at x=0.1 already. On the other hand, weaker deviations are found for the scattering parameters at this x range; however, for large x, they diverge much more strongly than the absorption coefficient.
To apply and extend the presented data, the reader is encouraged to use the MATLAB Functions given in the Appendix.

References

Bohren C.F. and D.R. Huffman, “Absorption and Scattering of Light by Small Particles”, John Wiley, New York, NY (1983).

Chandrasekhar S., "Radiative Transfer", Dover Publication (1960), BEWI TDD 211.

Deirmendjian, D. “Electromagnetic Scattering on Spherical Polydispersions”, American Elsevier, New York, NY (1969).

de Wolf D.A. “On the Laws-Parsons distribution of raindrop sizes”, Radio Science Vol.36, No. 4, pp. 639-642 (2001).

Ishimaru A., “Wave propagation and scattering in random media”, Vol. 1, Academic Press, Orlando, FL (1978).

Liebe H.J., G.A. Hufford and T. Manabe, “A model for the complex permittivity of water at frequencies below 1 THz”, Internat. J. Infrared and mm Waves, Vol. 12, pp. 659-675 (1991).

Liebe, H.J., G.A. Hufford, and M.G. Cotton, Propagation Modeling of Moist Air and Suspended Water/Ice Particles at Frequencies Below 1000 GHz. AGARD Conference Proc. 542, Atmospheric Propagation Effects through Natural and Man-Made Obscurants for Visible to MM-Wave Radiation, pp.3.1-3.10 (1993).

Math Works, “MATLAB User’s Guide”, Natick, MA (1992).

Mätzler C., “Radarsignale von anisotropem Niederschlag ”, IAP Res. Rep. No. 02-2, April (2002a).

Mätzler C., “MATLAB Functions for Mie Scattering and Absorption”, IAP Res. Rep. No. 02-08, June (2002b).

Mie G. “Beiträge zur Optik trüber Medien, speziell kolloidaler Metallösungen“, Annals of Physics, Vol. 25, pp. 377-445 (1908).

Meador W.E. and W.R. Weaver, “Two-Stream Approximations to Radiative Transfer in Planetary Atmospheres: A Unified Description of Existing Methods and a New Improvement”, J. Atm. Sciences, Vol. 37, pp. 630-643 (1980).

Olsen R.L., D.V. Rogers and D.B. Hodge, “The aR^b relation in the calculation of rain attenuation”, IEEE Trans. Ant. Prop. Vol. AP-26, pp. 318-329 (1978).

Ray P.S. “Broadband complex refractive indices of ice and water”, Applied Optics, Vol. 11, No. 8, pp. 1836-1844 (1972).

Sauvageot H., “Radar Meteorology”, Artech House, Boston, MA (1992).

van de Hulst H.C. “Light Scattering by Small Particles”, (1957), reprinted by Dover Publication, New York, NY (1981).

Appendix: The main MATLAB Functions

This appendix contains the main MATLAB routines used in this report. The routines make use of the Mie Functions defined elsewhere (Mätzler 2002b). Some additional routines are slight modifications of the ones shown here, e.g. to plot the temperature dependence of the coefficients or to compare with Rayleigh Theory.

A1 epswater

```
function result = epswater(fGHz, TK)

% Dielectric permittivity of liquid water without salt according to Liebe et al. 1991 Int. J. IR+mm Waves 12(12), 659-675
% Frequency range: 1 to 1000 GHz, temperature range: 270 to 310 K, extended 250 to 330 K
% Input: fGHz: frequency in GHz, TK: temperature in K
% Mätzler, June 2002

TETA=1-300/TK;
e0=77.66-103.3*TETA;
e1=0.0671*e0;
f1=20.2+146.4*TETA+316*TETA.*TETA;
e2=3.52+7.52*TETA;
% version of Liebe 1993 uses: e2=3.52
f2=39.8*f1;
eps=e2+(e1-e2)./(1-i*fGHz./f2)+(e0-e1)./(1-i*fGHz./f1);
result=eps;
```

A2 Mie_rain1

```
function result = Mie_rain1(fGHz, TK, nsteps, dD)

% Efficiencies of rain extinction, scattering, absorption backscattering and asymmetric scattering, using Mie Theory and
% the dielectric model of Liebe et al. (1991), see epswater.
% Input: fGHz frequency in GHz, TK temperature in K, nsteps number of diameters (D in mm), dD increment of D in mm
% C. Mätzler, June 2002

m=sqrt(epswater(fGHz, TK));
nx=(1:nsteps)';
D=(nx-1)*dD;
c0=299.793;
x=pi*D*fGHz/c0;
for j = 1:nsteps
   a(j,:)=Mie(m,x(j));
end;
output_parameters='Real(m), Imag(m), D, Qext, Qsca, Qabs, Qb, <costeta>'
a(:,3)=D;
m1=real(m);m2=imag(m);
plot(a(:,3),a(:,4:8))                          % plotting the results
legend('Qext','Qsca','Qabs','Qb','<costeta>')
title(sprintf('Mie Efficiencies for raindrops f=%gGHz, T=%gK,
m=%g+%gi',fGHz,TK,m1,m2))
xlabel('D (mm)'),   ylabel('Mie Efficiency')
result=a;
```

A3 Mie_rain2

```
function result = Mie_rain2(fGHz, TK, R)

% Weighting functions of  Rain extinction, scattering, absorption, backscattering and asymmetric scattering coefficient
```

```
%  in 1/km/mm versus drop diameter for Marshall-Palmer (MP) size distribution (Sauvageot et al. 1992)
% using Mie Theory, and dielectric model of Liebe et al. 1991. Input:
% fGHz: frequency in GHz, TK: Temp. in K, R: rain rate in mm/h
% C. Mätzler, June 2002.

nsteps=501; dD=0.01*R^(1/6)/fGHz^0.05;
% nsteps: number of D values, dD: drop-size interval in mm
m=sqrt(epswater(fGHz, TK));
N0=0.08/10000;              % original MP N0 in 1/mm^4
LA=4.1/R^0.21;
nx=(1:nsteps)';
D=(nx-1)*dD;
c0=299.793;
x=pi*D*fGHz/c0;
sigmag=pi*D.*D/4;
NMP=N0*exp(-LA*D);
sn=sigmag.*NMP*1000000;
for j = 1:nsteps
   a(j,:)=Mie(m,x(j));
end;
b(:,1)=D;
b(:,2)=a(:,4).*sn;
b(:,3)=a(:,5).*sn;
b(:,4)=a(:,6).*sn;
b(:,5)=a(:,7).*sn;
b(:,6)=a(:,5).*a(:,8).*sn;
m1=real(m);m2=imag(m);
plot(b(:,1),b(:,2:6))                              % plotting the results
legend('dGext/dD','dGsca/dD','dGabs/dD','dGb/dD','d(Gsca*<costeta>)/dD')
title(sprintf('Rain Effects at f=%gGHz, T=%gK, R=%gmm/h',fGHz,TK,R))
xlabel('D (mm)');ylabel('dGi/dD (1/km/mm)')
gext= sum(b(:,2))*dD;
gsca= sum(b(:,3))*dD;
gabs= sum(b(:,4))*dD;
gb=   sum(b(:,5))*dD;
gteta=sum(b(:,6))*dD;
result=[gext gsca gabs gb gteta];
```

A4 Mie_rain3

```
function result = Mie_rain3(fGHz, TK, nrain, pam)

% Extinction, scattering, absorption, backscattering and asymmetric scattering coefficients in 1/km versus rain rate,
% for Marshall-Palmer (MP) drop-size distribution (Sauvageot et al. 1992), using Mie Theory, and Liebe 91 dielectric model.
% Input: fGHz: frequency in GHz, TK: Temp. in K, nrain: Number of rain rates between Rmin=0.1 and Rmax=100mm/h
% pams: 0 if no costeta data to be given, 1 if they are needed
% C. Mätzler, June 2002.

Rmin=0.1;
nsteps=501;
m=sqrt(epswater(fGHz, TK));
N0=0.08/10000;              % original MP N0 in 1/mm^4
fact=1000^(1/(nrain-1));
R=Rmin/fact;
nx=(1:nsteps)';
c0=299.793;
for jr = 1:nrain
   R=R*fact;
   dD=0.01*R^(1/6)/fGHz^0.05;
   D=(nx-1)*dD;
```

```
   x=pi*D*fGHz/c0;
   sigmag=pi*D.*D/4;
   LA=4.1/R^0.21;
   NMP=N0*exp(-LA*D);
   sn=sigmag.*NMP*1000000;
   for j = 1:nsteps
      a(j,:)=Mie(m,x(j));
   end;
   b(:,1)=D;
   b(:,2)=a(:,4).*sn;
   b(:,3)=a(:,5).*sn;
   b(:,4)=a(:,6).*sn;
   b(:,5)=a(:,7).*sn;
   b(:,6)=a(:,5).*a(:,8).*sn;
   gext= sum(b(:,2))*dD;
   gsca= sum(b(:,3))*dD;
   gabs= sum(b(:,4))*dD;
   gb=   sum(b(:,5))*dD;
   gteta=sum(b(:,6))*dD;
   res(jr,:)=[R gext gsca gabs gb gteta];
end;
   if pam==0
      output_parameters='Gext, Gsca, Gabs, Gb'
      plot(res(:,1),res(:,2:5))
      legend('Gext','Gsca','Gabs','Gb')
      title(sprintf('Mie Propagation Coefficients Versus Rain Rate at f=%gGHz, T=%gK',fGHz,TK))
      xlabel('R (mm/h)');    ylabel('Gi(1/km)')
   elseif pam==1
      output_parameters='Gext, Gsca, Gabs, Gb, Gsca*<costeta>'
      plot(res(:,1),res(:,2:6))
      legend('Gext','Gsca','Gabs','Gb','Gsca*<costeta>')
      title(sprintf('Mie Propagation Coefficients Versus Rain Rate at f=%gGHz, T=%gK',fGHz,TK))
      xlabel('R (mm/h)');    ylabel('Gi(1/km)')
   end;
result=res;
```

A5 Mie_rain4

```
function result = Mie_rain4(R, TK, fmin, fmax, nfreq)

% Extinction, scattering, absorption, backscattering and
% asymmetric scattering coefficients in 1/km for Marshall-Palmer
% (MP) drop-size distribution (Sauvageot et al. 1992),
% versus frequency, using Mie Theory and dielectric Model of
% Liebe et al. 1991, Input:
% R: rain rate in mm/h, TK: Temp. in K,
% fmin, fmax: minimum and maximum frequency in GHz
% nfreq: Number of frequencies
% C. Mätzler, June 2002.

nsteps=501;
N0=0.08/10000;              % original MP N0 in 1/mm^4
fact=(fmax/fmin)^(1/(nfreq-1));
fGHz=fmin/fact;
nx=(1:nsteps)';
c0=299.793;
for jr = 1:nfreq
   fGHz=fGHz*fact;
   m=sqrt(epswater(fGHz, TK));
   dD=0.01*R^(1/6)/fGHz^0.05;
```

```
    D=(nx-1)*dD;
    x=pi*D*fGHz/c0;
    sigmag=pi*D.*D/4;
    LA=4.1/R^0.21;
    NMP=N0*exp(-LA*D);       % MP distribution
    sn=sigmag.*NMP*1000000;
    for j = 1:nsteps
       a(j,:)=Mie(m,x(j));
    end;
    b(:,1)=D;
    b(:,2)=a(:,4).*sn;
    b(:,3)=a(:,5).*sn;
    b(:,4)=a(:,6).*sn;
    b(:,5)=a(:,7).*sn;
    b(:,6)=a(:,5).*a(:,8).*sn;
    gext= sum(b(:,2))*dD;
    gsca= sum(b(:,3))*dD;
    gabs= sum(b(:,4))*dD;
    gb=   sum(b(:,5))*dD;
    gteta=sum(b(:,6))*dD;
    res(jr,:)=[fGHz gext gsca gabs gb gteta];
end;
output_parameters='Gext, Gsca, Gabs, Gb, Gsca*<costeta>'
plot(res(:,1),res(:,2:6))
legend('Gext','Gsca','Gabs','Gb','Gsca*<costeta>')
title(sprintf('Mie Propagation Coefficients Versus Frequency at R=%gmm/h, T=%gK',R,TK))
xlabel('f (GHz)');    ylabel('Gi(1/km)')
result=res;
```